

First-principles studies of FeS₂ using many-body perturbation theory in the G_0W_0 approximation

Timo Schena,* Gustav Bihlmayer, and Stefan Blügel

Peter Grünberg Institut and Institute for Advanced Simulation, Forschungszentrum Jülich and JARA, D-52425 Jülich, Germany

(Received 20 September 2013; published 10 December 2013)

We present a theoretical study on iron pyrite using density-functional theory (DFT) and the GW approximation to many-body perturbation theory. The fundamental band gap of iron pyrite is determined by iron $3d$ states at the valence band edge and a sulfur $3p$ -dominated conduction band at Γ . The gap is quite sensitive to structural changes as well as to the applied electronic structure method. We found that this p -dominated band does not play a significant role for the optical absorption, leading to a large difference between the optical and fundamental band gaps of iron pyrite. As a consequence the GW -corrected energies result in no considerable change of the optical band gap as compared to standard DFT, both being in reasonable agreement with experiment. However, we show that the fundamental band gap is reduced to about 0.3 eV in GW , which may contribute to the low open-circuit voltage of about 0.2 V observed in iron pyrite solar cells, representing a serious bottleneck for photovoltaic applications. To demonstrate that this unconventional reduction of the p - d gap is not unique for iron pyrite, similarities for FeS₂ in the marcasite structure are presented.

DOI: [10.1103/PhysRevB.88.235203](https://doi.org/10.1103/PhysRevB.88.235203)

PACS number(s): 71.15.Ap, 71.20.Nr, 78.20.Ci, 72.40.+w

I. INTRODUCTION

FeS₂ pyrite is known to be a promising photovoltaic material due to its large optical absorption coefficient of about $6 \times 10^5 \text{ cm}^{-1}$ and a suitable band gap of 0.95 eV.¹ Such a large optical absorption can lead to high quantum efficiency in thin films of only about 10 nm thickness, whereas ordinary Si films need to be at least 10–100 times thicker. There are experiments² showing n - as well as p -type conductivity in iron pyrite using suitable dopants as As, Ni, or Co, which may be of importance to assemble pn junctions for iron pyrite solar cells. Moreover, FeS₂ pyrite, consisting of abundant materials, would allow for large-scale and sustainable applications. However, all attempts using pyrite as optical absorber in solar cells have shown disappointing performances, yielding at maximum an open-circuit voltage of about 0.2 V.¹ Even lower open-circuit voltages have been measured in a recent work for pyrite nanocrystal solar cells.³

Many publications about pyrite focus on the possible reasons of the low open-circuit voltage. However, the mechanism is still unclear. Electrical resistivity measurements yield large free charge carrier densities in an order of 10^{14} – 10^{18} cm^{-3} in undoped pyrite, which is attributed to unspecified defects in the material.^{2,4} A first attempt to explain the low open-circuit voltage is based on the formation of sulfur vacancies in the bulk, leading to defect states in the band gap acting as charge recombination centers.⁵ The possibility of intrinsic surface states in the (100) surface giving rise to a Fermi level pinning has been also discussed.⁶ Both causes have been reported to be unlikely to explain the low open-circuit voltage due to a large formation energy of the sulfur vacancies in bulk⁷ and missing intragap surface states for the (100) surface.⁸ A very recent work by Herbert *et al.*⁹ claims, however, a band gap decrease to 0.4 ± 0.1 eV due to intrinsic surface states in the (100) surface using scanning tunneling spectroscopy measurements and simulations. The observed formation of the structurally related FeS₂ marcasite during synthesis may be also ruled out as a cause since experimental as well as DFT-based results indicate an at least as large band gap in FeS₂ marcasite and a similar strong optical absorption compared to

iron pyrite.^{8,10} Instead, Sun *et al.*⁷ proposed oxygen impurities acting as substitutional defects for sulfur as a possible cause of an unintentional p -type conductivity in pyrite reducing the device performance. However, Hu *et al.*^{11,12} showed a band gap increase for oxygen-alloyed pyrite, which may improve the carrier mobilities and lifetimes and therefore also the device performance. Furthermore, the same group suggested to use sulfur-poor conditions for the synthesis of pyrite thin films because sulfur-rich (100) surfaces might be responsible for the low open-circuit voltage due to small band gaps.¹³ Finally, the formation of metallic sulfur-poor FeS_x precipitates at the surface is also offered as a cause, worsening the performance of the pyrite solar cells.¹⁴

While most studies focus on the presence of defects or phase impurities, there are also electronic structure calculations showing that already in the ideal bulk structure the question of the precise band position of energy bands controlling the size of the fundamental band gap is still not settled. Eyert *et al.*¹⁵ demonstrated a rather sensitive dependence of the band gap in pyrite on structural parameters, claiming the large optical absorption is caused by transitions between the valence band maximum (VBM) Fe $3d$ states and the S $3p$ states at the conduction band minimum (CBM) around Γ . However, recent results of the pseudodielectric function by Choi *et al.*¹⁶ indicate that the optical transitions from the VBM to this p band are strongly suppressed. Therefore, optical measurements may be not able to detect the conduction band minimum and the fundamental band gap of pure pyrite might be much smaller than the optical band gap of 0.95 eV measured experimentally.¹ A very recent theoretical study by Lazić *et al.*¹⁷ supports this assumption. Experiments using temperature-dependent electrical resistivity measurements^{18,19} indicate an activation energy of around 0.2 eV, corresponding to a much smaller band gap of about 0.4 eV. However, it is unclear how strongly the results have been affected by defects in the material.

Most of the aforementioned publications are based on density-functional theory^{20,21} (DFT) calculations using the generalized gradient approximation (GGA) proposed by Perdew-Burke-Ernzerhof (PBE).²² In some cases an inclusion

of local Hubbard U corrections via the DFT + U method²³ has been used to consider correlation effects. However, comparing the experimental optical absorption of pyrite with the calculated optical absorption spectrum with and without U , Choi *et al.*¹⁶ report a worsening of the calculated spectrum after applying U . Moreover, it is well known that the (semi)local exchange-correlation functionals suffer from several practical and conceptual shortcomings in the description of semiconducting or insulating systems, usually leading to a severe underestimation of the band gap as compared to the experimentally observed one.^{24,25} Frequently, an improvement of the band gap description is achieved by more sophisticated orbital-dependent exchange-correlation functionals, such as the HSE06 hybrid functional.^{26,27} However, for the case of FeS₂ pyrite the band gap is drastically overestimated within HSE06 leading to values around 2.6 eV.^{8,16} To obtain a more systematic improvement of the band gaps, the GW approximation based on the many-body perturbation theory has proven to be a successful approach beyond conventional DFT.²⁸ Choi *et al.*¹⁶ briefly report about a reduction of the fundamental band gap of iron pyrite to 0.4 eV using the GW approximation, but almost not affecting the optical functions compared to conventional DFT results. On the other hand, there is one publication presenting the quasiparticle self-consistent GW band structure of pyrite,²⁹ yielding a band gap of 0.81 eV, which agrees well with the experimentally observed one. However, no optical absorption has been included in this comparison.

To our knowledge, there is no publication showing a systematic convergence analysis of the band gap of FeS₂ pyrite within the GW approximation with respect to the number of bands and local orbitals that improve the description of unoccupied bands and semi-core states. This paper indicates that it is quite subtle to converge the band gap of pyrite, similar to the situation in ZnO.^{30,31} In addition, the difference between the optical and fundamental band gaps in iron pyrite is analyzed by calculating the optical absorption. We also point out possible consequences for a reinterpretation of the experimentally measured band gap and the open-circuit voltage in iron pyrite. Moreover, no comparison of computational results for marcasite FeS₂ has been presented in the literature that would allow us to judge the performance of the methods for these iron compounds. FeS₂ marcasite is of particular interest because it may have an effect on the photovoltaic performance of iron pyrite solar cells, when forming during the synthesis of FeS₂ pyrite.

This paper is structured as follows: In Sec. II the structure of pyrite is introduced, followed by Sec. III presenting the computational details. In Sec. IV the electronic and optical properties of iron pyrite calculated via the PBE functional are shown, whereas in Sec. V the role of the quasiparticle corrections within the GW approximation is highlighted. In Sec. VI the results are discussed in detail, followed by a short analysis of the FeS₂ marcasite system in Sec. VII. Finally, in Sec. VIII we draw the major conclusions of our work.

II. PYRITE STRUCTURE

The iron pyrite structure is displayed in Fig. 1. The unit cell is simple cubic with $Pa\bar{3}$ space group containing 12 atoms.

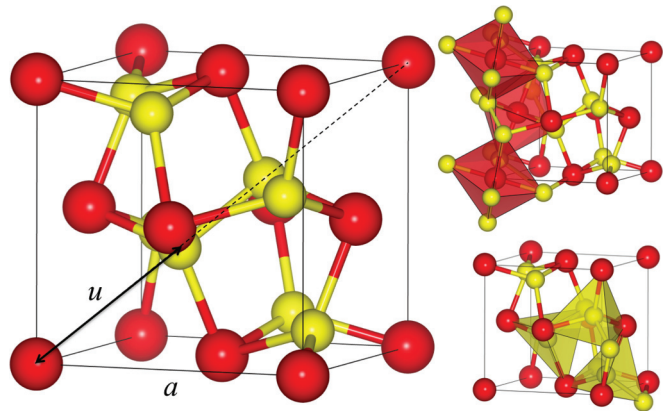


FIG. 1. (Color online) The iron pyrite structure with the S atoms indicated as light gray (yellow) spheres and the Fe atoms in dark gray (red) color. In the right panel the (almost) octahedral and tetrahedral coordination of the Fe and S atoms are displayed. The octahedrons share their corners. In the tetrahedrons the characteristic S dimers are clearly visible. The lattice constant a and the Wyckoff parameter u are the structural parameters mentioned in the text.

Characteristic for the pyrite structure are S dimers, which are orientated along the $\langle 111 \rangle$ directions. It can be seen as NaCl structure with the Fe atoms occupying the Na positions and the centers of the S dimers located at the Cl positions. Each Fe atom is almost octahedrally coordinated by neighboring S atoms, whereas each S atom has a tetrahedral surrounding, being bond to three Fe atoms and one additional S atom, together forming the S dimer. The distance of the S atoms in the S dimer is smaller than the distance between neighboring S and Fe atoms. The S dimer is a result of the formation of a strong covalent bond. This and the almost octahedral symmetry play a key role for the electronic structure, presented in Sec. IV. The structure can be described via a lattice parameter a and the Wyckoff parameter u , giving the internal positions of the S atoms in the unit cell (see Fig. 1). The distance between the S atoms in the S dimer is in a linear relation to the Wyckoff parameter via $d_{S-S} = \sqrt{3}a(1 - 2u)$. Thus, u has a strong influence on the electronic structure, as already pointed out by Eyert *et al.*¹⁵ Unless indicated otherwise, we used the experimentally determined lattice parameter and Wyckoff parameter with $a = 5.418 \text{ \AA}$ and $u = 0.385$.³² Experimentally there are variations of 0.5% for a and u , possibly due to defects.

III. COMPUTATIONAL DETAILS

We performed DFT (Refs. 20 and 21) calculations with the full-potential linearized augmented plane wave (FLAPW) method³³ using the generalized gradient approximation in PBE form²² as implemented in the FLEUR code.³⁴ The results have been carefully converged with respect to the number of \mathbf{k} points, the plane wave cutoff k_{\max} , as well as the maximal angular momentum quantum number l_{\max} in the expansion of the spherical harmonics of the LAPW basis functions in the muffin tin spheres with radii $R_{\text{MT}}^{\text{Fe}}$ and R_{MT}^{S} for Fe and S, respectively. We used at least $4 \times 4 \times 4$ \mathbf{k} points, $k_{\max} = 4.0 \text{ a.u.}^{-1}$, $R_{\text{MT}}^{\text{Fe}} = 2.23 \text{ a.u.}$, $R_{\text{MT}}^{\text{S}} = 1.98 \text{ a.u.}$, and $l_{\max} = 8$ for the PBE results. Bulk pyrite is nonmagnetic, and therefore the calculations have been carried out without spin polarization. A magnetic test

calculation converged against the nonmagnetic result. For the structural relaxation the forces have been converged to the order 10^{-5} htr/a.u.

The one-shot GW calculations, denoted by G_0W_0 , have been performed with the SPEX code³⁵ on top of the converged PBE results. The convergence of the transition energies in GW with respect to the numerical cutoff parameters is a much more subtle issue as compared to GGA calculations. Because also the wave functions of the unoccupied states are entering the GW calculations to construct the polarization function and the correlation self-energy, a proper description of these is essential for convergence. Therefore, depending on the system, many unoccupied bands have to be taken into account, leading to the necessity to use a large plane wave and spherical harmonic cutoff parameter. We increased the plane wave cutoff and the maximal angular momentum quantum number to $k_{\max} = 6.0$ a.u.⁻¹ and $l_{\max} = 12$. The muffin tin radii and \mathbf{k} points remain the same as in the above PBE calculation. Additionally, the linearization error of the FLAPW method needs to be reduced by using local orbitals in the unoccupied energy spectrum.^{31,36} Five unoccupied s , p , d , and f sets of local orbitals have been included, covering energies up to 800 eV, according to the high-energy local orbitals of Michalíček *et al.*,³⁷ i.e., 80 additional basis functions have been used per atom. To guarantee for the orthogonality of the core states on the LAPW basis for states below the Fermi level, as well as above, semi-core states possibly need to be included into the basis set. In contrast to the DFT calculations, the additional inclusion of the Fe $3s$ and $3p$ semi-core states as local orbitals has a considerable influence on the results. It has been shown that the overlap of these states with higher-lying states leads to a significant modification of the band positions in schemes using orbital-dependent functionals^{38,39} as well as in GW calculations.⁴⁰⁻⁴² A detailed convergence analysis for the GW results regarding the number of bands is presented in Sec. V.

The optical absorption is calculated by integration over a $20 \times 20 \times 20$ \mathbf{k} mesh and considering the transition matrix elements of the dipole operator using transitions up to about 6 eV. For partitioning the optical absorption into the contributions $\mathcal{A}_{\mu \rightarrow \nu}(\omega)$ coming from transitions between different orbital states μ and ν , we used

$$\mathcal{A}_{\mu \rightarrow \nu}(\omega) \sim \sum_{\mathbf{k}} \sum_{i,f} |\langle f | \hat{d} | i \rangle|^2 \delta[\omega - (\varepsilon_f - \varepsilon_i)] \rho_f^{\nu} \rho_i^{\mu}, \quad (1)$$

where i and f are the initial and final states with the corresponding energies ε_i and ε_f and orbital contributions ρ_i^{μ} and ρ_f^{ν} in orbital μ and ν , and \hat{d} the electric dipole operator.

IV. GGA RESULTS

The electronic band structure of iron pyrite using the experimental lattice constant $a = 5.418$ Å and Wyckoff parameter $u = 0.385$ is displayed in the left panel of Fig. 2 along a high-symmetry \mathbf{k} path. In the right panel the corresponding density of states (DOS) partitioned into the S $3s$ -, S $3p$ -, and Fe $3d$ -orbital contributions is presented. The electronic structure can be quite easily understood regarding the geometrical characteristics of the pyrite structure, as presented in Sec. II. First of all, the strong covalent bonds of the S dimers cause

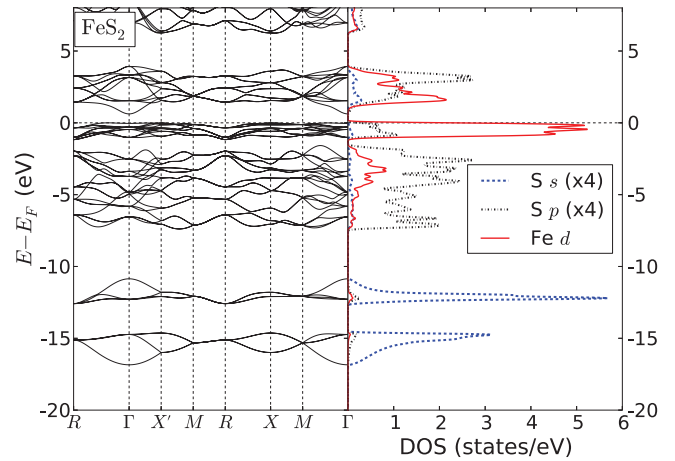


FIG. 2. (Color online) The DFT band structure of pyrite (left) and the corresponding LDOS (right) characterized into S $3s$ - (blue dashed line), S $3p$ - (black pointed line), and Fe $3d$ -orbital contributions (red solid line). The S $3s$ and S $3p$ LDOS is enhanced by a factor of 4.

the formation of bonding and antibonding ss and pp orbitals. Between -17 to -10 eV, the S $ss\sigma$ and $ss\sigma^*$ states are located, well separated from the S $pp\sigma$, $pp\pi$, and $pp\pi^*$ states ranging from -7 to -2 eV. The closer the states are to the Fermi energy, the more they are hybridizing with Fe $3d$ states. Due to the almost octahedral coordination of the neighboring S atoms around Fe, crystal field splitting separates the Fe $3d$ t_{2g} and e_g states around the Fermi level. Notice that the t_{2g} and e_g labels do not relate to the global z axis, but to the canted principal axes of the octahedrons of the crystal. The Fe $3d$ t_{2g} states are localized ranging from -2 eV to the Fermi energy and show some hybridization with S $3p$ states, whereas the Fe $3d$ e_g states start at around 1 eV reaching to 4 eV. The hybridization between the Fe e_g states and the S $pp\sigma^*$ states is quite strong in the conduction bands. However, a single almost entirely p -like conduction band is approaching the Fermi energy at Γ , defining the fundamental band gap in iron pyrite. Within the experimental structural setup FeS₂ pyrite exhibits an indirect fundamental band gap of 0.62 eV size. The direct band gap at Γ is slightly larger with 0.66 eV. The orbital-character-resolved fat-band structure of iron pyrite in Fig. 3, with the S $3p$ character in black and the Fe $3d$ character in red color, illustrates this point. Exactly at Γ the wave function of the VBM exhibits pure Fe $3d$ character, whereas the CBM consists purely of S $3p$. But also in the vicinity of Γ the orbital characters are very pure, leading to dramatic consequences for the optical absorption, as it will be discussed later.

This distinct orbital behavior in FeS₂ pyrite has been pointed out already in other works.^{12,15} Eyert *et al.*¹⁵ discussed the delicate dependence of the position of the p -like band on the Wyckoff parameter u : since u is linearly related to the distance of the S atoms in the S dimer, it controls the splitting between the bonding and antibonding $pp\sigma$ states. Optimizing the pyrite structure by energy minimization exhibits a lattice constant of $a = 5.403$ Å and a Wyckoff parameter $u = 0.383$. For a smaller u the distance between the S atoms in the S dimer increases, leading to a smaller band gap. With 0.39 eV the band gap in iron pyrite using the relaxed structure is around 0.2 eV

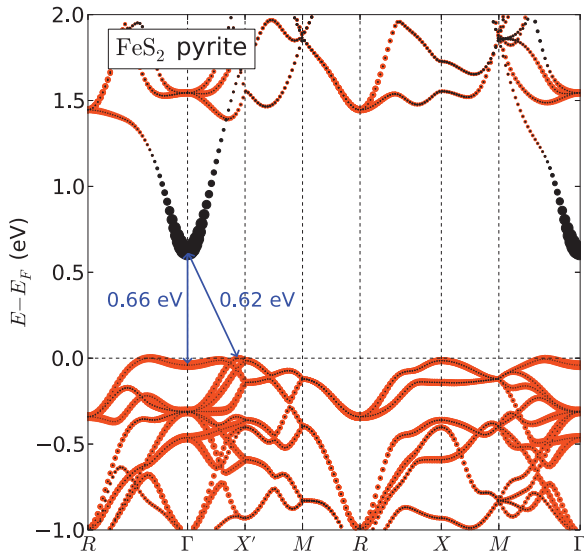


FIG. 3. (Color online) The orbital-resolved band structure of iron pyrite along a high-symmetry k path for the experimentally determined structural parameters $a = 5.418 \text{ \AA}$ and $u = 0.385$. The high-symmetry points are denoted according to Bradley and Cracknell (Ref. 43), with X' being equivalent to X . The direct band gap at Γ with 0.66 eV is slightly larger than the indirect one with 0.62 eV . The band structure of pyrite shows a clear d -like behavior in the VBM regime and in the region of the localized bands in the conduction band originating from Fe indicated in gray (red), whereas a delocalized p state coming from sulfur dominates at Γ (indicated in black). Fat points indicate a strong contribution of the corresponding orbital character.

smaller than the structure with the experimental parameters. The change in the lattice parameter has almost no impact on the gap size. The band gap of the relaxed structure is in excellent agreement with other published DFT results.^{8,13} Vidal *et al.*⁴⁴ observed a strong dependence of the band gap in $\text{CuIn}(\text{S},\text{Se})_2$ on the internal structural parameter, which in turn is influenced by the Cu vacancy concentration, making it necessary to use a self-consistent approach. In iron pyrite the situation is, however, different since the S- and Fe-vacancy formation energy is much larger than the band gap.⁷

The calculated optical absorption within PBE is displayed in Fig. 4. The result, predicting two peaks, one at around 2 eV (peak A) and one at 3.5 eV (peak C), is in reasonable agreement with the experimentally observed optical absorption. The experimentally determined peak positions vary from around 1.6 to 2.3 eV for the first and 3.8 – 4.7 eV for the second peak.^{45–49} The first peak is always sharper and larger in intensity than the second peak. The peak positions of the optical absorption measured by Ferrer *et al.*⁴⁶ are indicated as black dashed lines in the inset of Fig. 4. In our theoretical calculations we can distinguish two additional peaks B and D. We have analyzed the major contributions to these peaks by partitioning the optical absorption into the contributions coming from transitions between $\text{Fe } 3d \rightarrow 3d$, $\text{S } 3p \rightarrow 3p$, $\text{S } 3p \rightarrow \text{Fe } 3d$, and $\text{Fe } 3d \rightarrow \text{S } 3p$ states. All other orbital characters play a negligible role for the optical absorption up to 6 eV transition energy. We amplified the orbital contributions (by factors of about 22, 150, 74, and 57, respectively) to yield

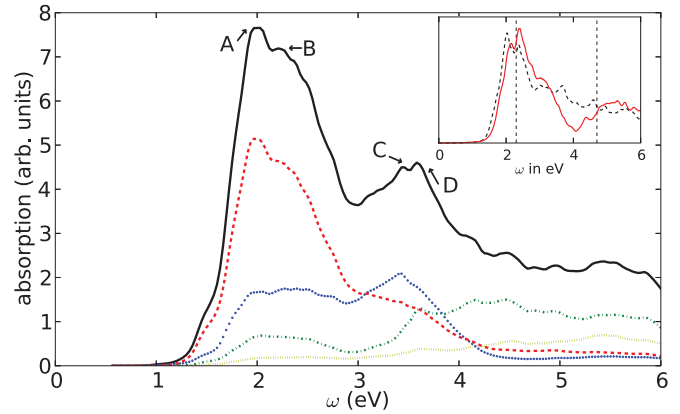


FIG. 4. (Color online) The optical absorption of iron pyrite depending on the photon energy is displayed for a calculation within PBE (black solid curve). To analyze the orbital contributions of the peaks A, B, C, and D, the optical absorption has been partitioned into $\text{Fe } 3d \rightarrow 3d$ (red dashed curve), $\text{S } 3p \rightarrow 3p$ (yellow striped curve), $\text{S } 3p \rightarrow \text{Fe } 3d$ (green dashed-dotted curve), and $\text{Fe } 3d \rightarrow \text{S } 3p$ contributions (blue dotted curve) as explained in the text. In the inset the optical absorption calculated on a coarse $4 \times 4 \times 4$ k mesh is displayed within plain PBE (black dashed curve) and within G_0W_0 (red solid curve). The black dashed lines indicate the peak positions of the experimentally measured optical absorption by Ferrer *et al.* (Ref. 46).

approximately the total optical absorption up to 6 eV transition energy when summed up.⁵⁰ First of all, one would expect a large contribution arising at and around Γ from transitions between the $\text{Fe } 3d$ states at the VBM and the p -like band at the CBM due to clearly fulfilled dipole selection rules $\Delta l = 1$, as it is also stated by Eyert *et al.*¹⁵ But interestingly these transition elements almost do not contribute to optical absorption because the corresponding wave functions are localized on different atoms. Moreover, the transition elements between the topmost valence band and lowest conduction band along the k path $\Gamma \rightarrow X$ are exactly zero due to symmetry up to the band crossing where the orbital character of the lowest conduction band changes (see Fig. 3). Hence, the first major peak A at a photon energy of about 2 eV and also the second peak B at about 2.3 eV consist mainly of transitions between the $\text{Fe } 3d$ t_{2g} and e_g states at the respective band edges. If we talk about transitions between $\text{Fe } 3d \rightarrow 3d$ states, it is a simplified denotation for transitions between $\text{Fe } 3d$ -dominant states, showing a considerable hybridization with $\text{S } 3p$ states and therefore also fulfilling the electrical dipole selection rules. Hence, the optical band gap is mainly determined by $\text{Fe } 3d \rightarrow 3d$ transitions, whereas the fundamental band gap is defined by the position of the p band at the CBM. Therefore, the fundamental and optical band gap in iron pyrite can be quite different in size and character. For the two peaks C and D at around 3.5 and 3.6 eV , the contributions from transitions between $\text{S } 3p \rightarrow \text{Fe } 3d$ and $\text{Fe } 3d \rightarrow \text{S } 3p$ states become important. For larger transition energies than 4 eV also the $\text{S } 3p \rightarrow 3p$ transitions play a role.

V. G_0W_0 RESULTS

On top of our converged PBE results using the experimentally determined structural parameters, we performed G_0W_0

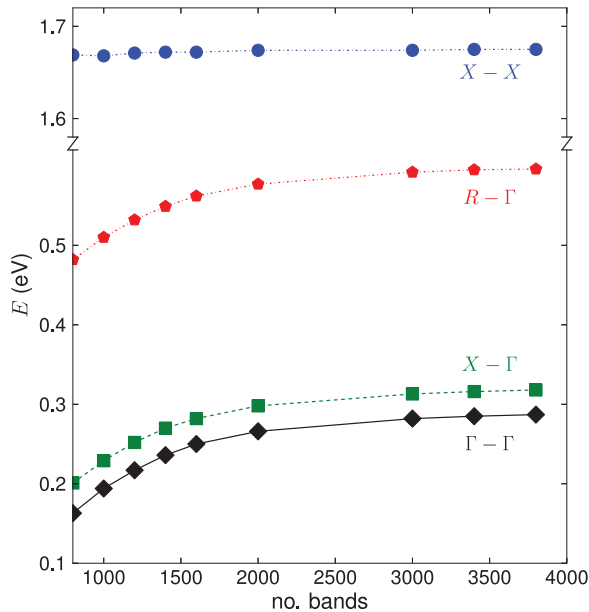


FIG. 5. (Color online) The transition energies between the band edges for the transitions $\Gamma \rightarrow \Gamma$ (black diamonds), $X \rightarrow \Gamma$ (green squares), $R \rightarrow \Gamma$ (red pentagons), and $X \rightarrow X$ (blue circles) are presented depending on the total number of bands for the single-shot G_0W_0 calculation. The G_0W_0 calculation has been performed on top of the converged PBE results using the structural parameters taken from experiment.

calculations using the SPEX code.³⁵ As explained in Sec. III, as compared to plain PBE calculations the convergence of the GW results is much more subtle, requiring large plane wave cutoffs and many local orbitals. We have analyzed the convergence for four different transitions, $\Gamma \rightarrow \Gamma$, $X \rightarrow \Gamma$, $R \rightarrow \Gamma$, and $X \rightarrow X$, with respect to the total number of bands. The results are presented in Fig. 5. The three transitions that include the Γ point in the conduction band exhibit a change from Fe $3d$ character to S $3p$ character, whereas the transition $X \rightarrow X$ is a transition between Fe $3d$ states. The transition $X \rightarrow X$ converges quite fast with respect to the number of bands, showing a convergence of the results to about 0.01 eV for 800 bands. However, the transitions including a change in orbital character need much more bands to reach convergence. As it can be seen in Fig. 5 around 2000–3000 bands are needed to obtain a similar convergence. This resembles the situation in ZnO, where 3000–4000 bands had been necessary to obtain convergence of the quasiparticle band gap that included a change in orbital character.^{30,31} The GW corrections in energy for the p -like state at Γ are almost independent of the number of bands and quite small, in the order of 0.01 eV, however, the quasiparticle correction for the d states delicately depends on the number of bands. Therefore, the transition $X \rightarrow X$ converges fast only due to a cancellation of systematic errors, i.e., the GW corrections of the d states in the conduction and valence band are of the same order and sign.

Comparing the transition energies in PBE and GW we find for the $X \rightarrow X$ transition a small increase of the gap energy from around 1.62 to 1.67 eV (Table I). An increase of the GW -corrected transition energy in comparison to the plain PBE result is rather expected and consistent with

TABLE I. Listed are the transition energies (units in eV) of iron pyrite for $\Gamma \rightarrow \Gamma$, $X \rightarrow \Gamma$, $R \rightarrow \Gamma$, and $X \rightarrow X$ transitions for the PBE and G_0W_0 calculation. For the G_0W_0 results converged values with 3000 bands have been used. For comparison, the G_0W_0 results with (w) and without (o) Fe $3s$ and $3p$ local orbital (LO) treatment are displayed.

	$\Gamma \rightarrow \Gamma$	$X \rightarrow \Gamma$	$R \rightarrow \Gamma$	$X \rightarrow X$
PBE	0.66	0.63	0.96	1.62
G_0W_0 (w Fe $3s$, $3p$ LOs)	0.28	0.31	0.59	1.67
G_0W_0 (o Fe $3s$, $3p$ LOs)	0.61	0.63	0.90	1.72

the conventional wisdom that the DFT employing local and semilocal exchange-correlation functional underestimates the band gap. However, quite surprisingly, for the transitions $\Gamma \rightarrow \Gamma$, $X \rightarrow \Gamma$, and $R \rightarrow \Gamma$ the gaps become considerably smaller. The energy of the transition $X \rightarrow \Gamma$ reduces from 0.63 to 0.31 eV applying the quasiparticle corrections. Using the PBE-structurally optimized atomic setup leads even to an almost metallic system with a small band gap of 0.05 eV. As can be seen from Fig. 3, the fundamental band gap occurs between the CBM at Γ and the VBM at a point in the $\Gamma \rightarrow X$ direction. Since the valence band states at the Fermi level are rather flat d bands, the $X \rightarrow \Gamma$ transition is energetically quite close to the fundamental band gap and reflects the behavior of the latter. Interestingly, the treatment of the Fe $3s$ and $3p$ semi-core states as local orbitals has a strong effect on the transition energies in the GW approximation. The results obtained without that treatment are quite different for $\Gamma \rightarrow \Gamma$, $X \rightarrow \Gamma$, and $R \rightarrow \Gamma$, leading to about 0.3 eV larger gaps.

Since the most crucial GW corrections take place around Γ , we present the band structure of iron pyrite along the k path $R \rightarrow \Gamma \rightarrow X'$ in Fig. 6, comparing the plain PBE results with the GW -corrected ones. The energy gap between the Fe $3d$ states is slightly increased, whereas the p state at Γ significantly drops down, reducing the fundamental band gap by about 0.3 eV. The effective mass of the CBM at Γ is enhanced in the GW calculation to $0.68 m_e$ from previous $0.48 m_e$ predicted within PBE. Hence, also the electronic mobility is increased by about 50%. The result of our GW -corrected band gap is in reasonable agreement with the result by Choi *et al.*¹⁶ reporting a value of 0.4 eV. However, it is not quite clear from that reference whether they used the pseudopotential of Fe with or without $3s$ and $3p$ semi-core states and what computational parameters had been chosen.

Using the GW -corrected energies leads to some significant changes of the optical absorption as it can be seen in the inset of Fig. 4. The one-shot G_0W_0 approximation of many-body perturbation theory does not alter the wave functions and therefore the matrix elements of the optical absorption are unchanged and the difference in the curves reflects just the shift in the eigenvalues. Due to the large shift of the p states with respect to the d states, the peaks C and D come much closer to the peaks A and B. The peaks start overlapping and the region from 2.5 to 4 eV looks quite different as compared to PBE and experiment. The PBE result is in a better agreement with experiment, however, due to the small corrections of the transition energies between the Fe $3d$ states the optical band gap is not changing much.

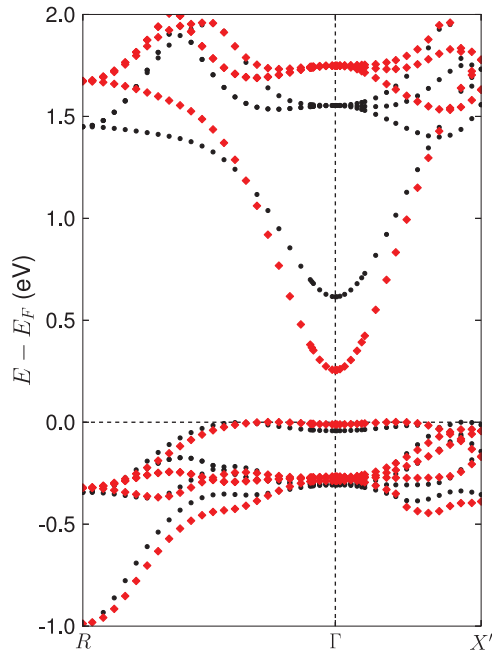


FIG. 6. (Color online) The band structure of iron pyrite for the high-symmetry k path $R \rightarrow \Gamma \rightarrow X'$ within PBE (black dots) and G_0W_0 (red diamonds). For both calculations the structural parameters from experiment have been used. Only the topmost five valence bands and five lowest conduction bands are displayed.

A negative band gap correction for $G_0W_0@PBE$ is rather unexpected since (semi)local exchange-correlation functionals tend to an underestimation of the fundamental band gap. However, a negative gap correction within G_0W_0 is not *per se* impossible and has been observed already in other cases.⁵¹ The opening of the gap is based on experience of employing GW to simple semiconducting systems, which usually exhibit either the same atomic or orbital character at the band edges, defining the band gap. In iron pyrite the self-energy correction is quite different for the S $3p$ state at the CBM and the Fe $3d$ states at the VBM, due to different local surroundings. In our case the negative gap correction might be caused by the large screening effects of the Fe $3d$ states, as it is also reported to a less dramatic extent for some half-metallic Heusler compounds.⁵² In a simplified way the GW correction in the self-energy can be divided into a contribution correcting the exchange Σ_{ex} and one considering the corrections in correlation Σ_{cor} , which is mainly due to screening. Σ_{ex} leads to an increase of the band gap, whereas on the other hand Σ_{cor} reduces the size of the gap. Usually Σ_{ex} is considerably larger than Σ_{cor} , leading to an overall increase of the band gap compared to the PBE one. However, large screening effects may lead to a small enhancement of the gaps or even to a reduction. To get an indication for our assumption, we compared the electronic structure of FeS₂ pyrite to isoelectronic RuS₂ and OsS₂ pyrites, which yield an almost unchanged band gap: comparing PBE and $G_0W_0@PBE$ we obtain 0.12 and 0.14 eV for RuS₂ and 0.75 and 0.80 eV for OsS₂, respectively. The decreasing localization of the cation d states for RuS₂ and OsS₂ at the band edges leads to smaller screening effects. Hence, the gap correction within GW becomes more positive.

VI. DISCUSSION

Our PBE results are in an overall nice agreement with the results of other theoretical work.^{8,16} The optical absorption spectra calculated within PBE properly describe the measured ones in iron pyrite. At first sight this is surprising because PBE is known to severely underestimate the band gaps in semiconductors. A good agreement of the optical absorption calculations with experiment can be expected from beyond-DFT calculations, e.g., time-dependent DFT or GW . However, the optical band gap in iron pyrite is defined mainly by transitions between the Fe $3d$ states at the VBM and Fe $3d$ states in the conduction band. The energy gap between these states does not show significant changes upon inclusion of the GW correction (see inset of Fig. 4). Having obtained a reasonable description within GGA and G_0W_0 , we now refer to HSE06 and DFT + U results for pyrite. Both methods have earned some merits in first-principles calculations for semiconductors and insulators. Surprisingly, the hybrid functional HSE06 (Refs. 26 and 27) drastically overestimates the transition energies between the d states at the VBM and the d states in the conduction band for iron pyrite. We have performed HSE06 calculations using the FLEUR code,⁵³ yielding about 3.8 eV as transition energy between the Fe $3d$ states at the VBM and the Fe $3d$ states at the conduction band edge and about 2.2 eV as fundamental band gap in iron pyrite. These values are in reasonable agreement with the results reported by Sun *et al.*⁸ and Choi *et al.*¹⁶ It seems that the strong electronic screening in iron pyrite due to the Fe $3d$ states at the VBM leads to wrong predictions using HSE06. In this case a modified screened-exchange HSE (Ref. 54) is known to be a better choice, where the Hartree-Fock exchange is not mixed with a factor of $\frac{1}{4}$, but $\frac{1}{\epsilon_0}$ into the exchange-correlation energy, with ϵ_0 being the static dielectric constant of the material. For iron pyrite the calculated static dielectric constant is about 20, leading to an almost plain GGA-like exchange-correlation energy within screened-exchange HSE, and therefore restoring the agreement of the optical properties with experiment. In contrast, a DFT + U treatment with a Hubbard- U parameter of $U = 2.4$ eV applied to the Fe d states and calculated using the constrained random-phase approximation⁵⁵ (c-RPA) worsens the agreement between theory and experiment in the optical absorption, shifting some of the peaks by more than 0.5 eV as compared to GGA.¹⁶ This behavior is a direct consequence of shifting the Fe $3d$ bands in the valence region downwards via the Hubbard- U parameter, whereas the Fe $3d$ bands in the conduction region are shifted upwards. Since the fundamental band gap of around 0.9 eV calculated within DFT + U seems to be in excellent agreement with the experimental value of 0.95 eV, the method has been interpreted to be the best to describe iron pyrite. However, due to the possibly significant difference between fundamental and optical band gap, the DFT + U results should be regarded critically. We have also performed an exact-exchange calculation within an optimized effective potential (EXX-OEP) as implemented in the FLEUR code,^{39,56} exhibiting a fundamental band gap of 2.7 eV for iron pyrite.

The optical absorption in iron pyrite is mainly determined by the position of the Fe $3d$ states, whereas for the fundamental band gap the position of the S p -like band at Γ relative

to the Fe 3*d* bands at the VBM is of crucial importance. Unfortunately, we are not able to affirm with full certainty whether the prediction of the fundamental band gap in iron pyrite within G_0W_0 is reliable since the first peaks of the calculated optical absorption spectra within G_0W_0 and GGA both are in reasonable agreement with experiment (see inset of Fig. 4), i.e., also the optical band gap is quite similar for both cases. Moreover, we observe a strong dependence of the results on the inclusion of Fe 3*s* and 3*p* semi-core states (see Table I). Usually, treating these states as local orbitals yields a more accurate description of the high-lying energy spectrum.

Finally, we compare to the quasiparticle self-consistent GW calculation performed by Lehner *et al.*²⁹ The fundamental band gap becomes larger (0.8 eV) than the GGA result, whereas for the optical absorption we would not expect large differences regarding the energy gap between the Fe 3*d* states at the band edges in the published band structure.²⁹ Since the quasiparticle self-consistent GW result of the fundamental band gap in iron pyrite is much larger than the G_0W_0 @PBE result with 0.3 eV, we have to expect a starting point dependence of the one-shot GW calculations, as reported in many references.^{57–59} We have conducted G_0W_0 calculations on top of PBE + U results. However, we observe an almost starting point independent behavior for a range of reasonable U values from 0 to 4 eV, leading to a prediction of 0.3–0.4 eV for the direct ($\Gamma \rightarrow \Gamma$) gap. For U values above 2.4 eV, the orbital character of the upmost valence band changes from almost pure Fe 3*d* character to considerably hybridized Fe 3*d* and S 3*p* states due to an exchange of bands. That and the connection to the quasiparticle self-consistent GW results may be of particular interest.

Therefore, also here we are not able to evaluate whether the quasiparticle self-consistent GW calculation is more reasonable than G_0W_0 or GGA. In addition, it is still an open question as to whether self-consistent GW methods lead to a deterioration of the spectral features as compared to one-shot GW methods, as it has been first shown for the homogeneous electron gas model by Schindlmayr *et al.*⁶⁰ It also has been reported that in some cases G_0W_0 tends to underestimate the band gap, while self-consistent GW methods lead to an overestimation of that quantity.⁶¹ Hence, further studies on the quasiparticle self-consistent GW results for transition metal chalcogenides need to be conducted in future.

As consequence, we can conclude that the position of the S 3*p*-rich band at Γ related to the localized Fe 3*d* states at the VBM and in the conduction band regime is not fully resolved. The disappointing performance of solar cells using iron pyrite as optical absorber could be caused not only by defects or precipitates, but also by the electronic structure of pristine FeS₂. If the p -like band determines the fundamental band gap of iron pyrite to be about 0.3 eV, this could explain the low open-circuit voltage. Due to the large difference in the Fe 3*d* \rightarrow 3*d* and Fe 3*d* \rightarrow S 3*p* matrix elements of the optical dipole operator, the available optical measurements based on the analysis of the optical absorption may be not able to get the limiting gap in iron pyrite. Measuring the position of the p -like band could be quite difficult. This single band does not contribute much to the density of states making it difficult to obtain the band gap with (inverse) photoemission spectroscopy, scanning tunneling microscopy, or two-photon

photoemission spectroscopy. Electrical resistivity measurements do not allow to discriminate easily different sources causing large free charge carrier densities and small resistivity since they are very sensitive to small impurity traces in the samples. Nevertheless, we can say that a measured intrinsic charge carrier density^{2,4} of about 10^{14} – 10^{18} cm⁻³ and an activation energy^{18,19} of around 0.2 eV can be explained very naturally by considering an optically inactive fundamental band gap of around 0.3 eV.

To investigate the role of the p band on the fundamental band gap in an experiment, one could think about shifting the p band to alter the gap. Hu *et al.* proposed to alloy iron pyrite with oxygen, leading to more localized $pp\sigma^*$ wave functions and therefore reducing the bandwidth of the $pp\sigma^*$ states.¹² However, it is not clear which oxygen doping concentrations can be achieved experimentally and how stable these alloys are. Another possibility to enhance the fundamental band gap could be to decrease the S-dimer distance by stress. A smaller S-dimer distance leads to a larger splitting of the $pp\sigma$ states and the p -like band may be shifted up with respect to the d states. However, it is unclear in which way stress influences the other bondings in iron pyrite and what are the consequences for the electronic structure.

VII. ANALOGY IN FeS₂ MARCASITE

Iron pyrite is not the only system that shows a sensitive p - d transition leading to peculiar results for GGA, HSE06, and GW calculations. With FeS₂ marcasite we have investigated a compound chemically related to iron pyrite, which is possibly forming during the synthesis of FeS₂ pyrite due to the complex phase diagram. In FeS₂ marcasite each Fe atom is also octahedrally coordinated to the S atoms, only this time the octahedrons share their edges. Again, the strong covalent bondings between the S atoms in S dimers have a large influence on the electronic structure. The unit cell of FeS₂ marcasite, displayed in the inset of Fig. 7, is an orthorhombic one, described by the lattice constants a , b , and c . The internal parameters u and v give the positions of the S atoms in the unit cell. The unit cell contains 6 atoms. We have used the experimental structure parameters of Brostigen *et al.*⁶² with $a = 4.443$ Å, $b = 5.424$ Å, $c = 3.387$ Å, $u = 0.200$, and $v = 0.378$. For the computation within PBE we used 64 k points for the Brillouin zone and a plane wave cutoff of $k_{\max} = 3.9$ a.u.⁻¹. The G_0W_0 calculations have been performed with a sufficiently large plane wave cutoff $k_{\max} = 7.0$ a.u.⁻¹, 2000 bands, and five full s , p , d , and f local orbital sets, i.e., 80 additional local orbital per atom. To improve the orthogonality of the LAPW basis functions on the core states, the Fe 3*s* and 3*p* states have been treated as semi-core local orbitals.

In the left panel of Fig. 7 the orbital-resolved band structure is presented along a high-symmetry k path. The valence bands and the majority of the conduction bands are dominated by Fe 3*d*-orbital character (indicated in red). Similar to iron pyrite the S 3*p* character (indicated in black) becomes dominant at Γ in one single band. However, in contrast to iron pyrite the fundamental band gap is determined by Fe 3*d*-rich conduction band states at T in PBE. Hence, the fundamental band gap is defined by Fe 3*d*–Fe 3*d* transitions and not between Fe 3*d* and S 3*p* states as in pyrite. Therefore, the numerical difficulties

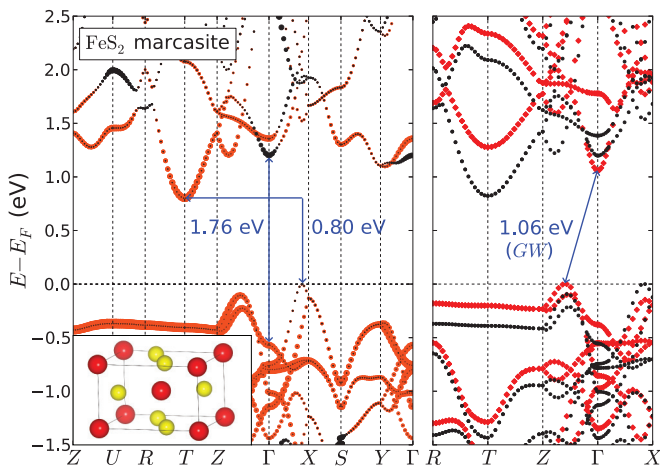


FIG. 7. (Color online) Left panel: The orbital-resolved band structure of FeS₂ marcasite for the experimental structural parameters within GGA. The high-symmetry points are denoted according to Bradley and Cracknell (Ref. 43). The Fe 3*d*-orbital character is indicated in gray (red), whereas the S 3*p*-orbital character is shown in black as in Fig. 3. Fat points indicate a strong contribution of the corresponding orbital character. The indirect band gap with 0.80 eV is much smaller than the direct transition at Γ with 1.76 eV. In the inset the unit cell of marcasite is displayed with the Fe atoms as dark gray (red) spheres and the S atoms in light gray (yellow). Right panel: The band structure of iron marcasite within PBE (black dots) and G_0W_0 (red diamonds). For the band structure, less k points have been used than for the transition energies of Table II, leading to small differences of the values in the order of 0.01 eV.

and the odd behavior for the GW -corrected results may not become visible in marcasite. Nevertheless, the same behavior can be observed when focusing on the transitions from the valence band to Γ in the conduction band. The transition energies for $\Gamma \rightarrow \Gamma$, $X \rightarrow \Gamma$, $R \rightarrow \Gamma$, and $X \rightarrow T$ within PBE and G_0W_0 are presented in Table II. Similar to the case in iron pyrite, the 3*d*-3*d* transition, here $X \rightarrow T$, is enhanced by GW , however, the correction is much larger than in the pyrite case. All transitions to Γ become smaller than PBE because the *p*-like band shifts downwards with respect to the *d* states. Overall, this leads to an increase of the fundamental band gap size from about 0.80 to 1.06 eV, as it can be seen in the right panel of Fig. 7, displaying the band structure of FeS₂ marcasite calculated within G_0W_0 . Hence, when focusing only on the size of the fundamental band gap, FeS₂ marcasite seems to behave rather normally in the GW approximation as

TABLE II. Listed are the energies (in eV) for FeS₂ marcasite of the transitions $\Gamma \rightarrow \Gamma$, $X \rightarrow \Gamma$, $R \rightarrow \Gamma$, and $X \rightarrow T$ for the PBE and G_0W_0 calculation. For the G_0W_0 results converged values with 2000 bands have been used. For comparison, the G_0W_0 results with (w) and without (o) Fe 3*s* and 3*p* local orbital (LO) treatment are displayed.

	$\Gamma \rightarrow \Gamma$	$X \rightarrow \Gamma$	$R \rightarrow \Gamma$	$X \rightarrow T$
PBE	1.76	1.32	1.57	0.95
G_0W_0 (w Fe 3 <i>s</i> , 3 <i>p</i> LOs)	1.40	1.19	1.21	1.40
G_0W_0 (o Fe 3 <i>s</i> , 3 <i>p</i> LOs)	1.88	1.57	1.72	1.25

compared to iron pyrite. Additionally, the band edges defining the fundamental band gap change, from the VBM located at a point near X and the CBM at T in PBE to the VBM at about Z and the CBM at Γ within G_0W_0 . Therefore, the character of the fundamental band gap changes from an Fe 3*d*-Fe 3*d* transition to an Fe 3*d*-S 3*p* transition as in iron pyrite. The local orbital treatment of the Fe 3*s* and 3*p* states is again crucial, leading to quite different results as displayed in Table II.

To conclude, also in FeS₂ marcasite a *p*-*d* transition plays a crucial role for the fundamental band gap, being quite sensitive to structural changes and the calculation method. Unfortunately, to our knowledge there are no high-quality measurements for the band gap and the optical properties of FeS₂ marcasite yet, despite a recent work indicating that FeS₂ marcasite has a band gap at least as large as that in FeS₂ pyrite.¹⁰ However, we expect the same discrepancies concerning the optical and fundamental band gaps as in iron pyrite. In addition to FeS₂ marcasite and iron pyrite, there are quite a lot of systems, which exhibit the same key features at the band edges, e.g., other isoelectronic pyrite- and marcasite-type compounds such as FeSe₂, FeTe₂, RuS₂, or OsS₂, but also β -FeSi₂. A careful analysis of this peculiar *p*-*d* interaction may be necessary for these systems.

VIII. CONCLUSIONS

We have presented first-principles results of iron pyrite using the FLAPW method as implemented in the FLEUR code.³⁴ Within the generalized gradient approximation we obtain a fundamental indirect band gap of about 0.62 eV, formed by a S 3*p*-rich conduction band at Γ and Fe 3*d* states at the valence band edge. The optical absorption in iron pyrite is dominated by transitions between Fe 3*d* states of the valence band and conduction band edges. Surprisingly, although the dipole selection rule $\Delta l = 1$ is fulfilled, the *p*-like band does not significantly contribute to optical absorption. These results are in nice agreement with results reported by other groups.^{8,16} To account for electronic excitations, we conducted G_0W_0 calculations as implemented in the SPEX code.³⁵ The fundamental band gap decreases to about 0.3 eV, showing the importance of the position of the *p*-like band at Γ with respect to the Fe 3*d* states. By presenting analogies in FeS₂ marcasite, we demonstrated the general importance of an accurate description of that position for a class of systems.

A detailed convergence analysis has shown the importance of a proper description of the wave functions in the unoccupied energy spectrum. This has been achieved by considering about 2000–3000 bands calculated within a sufficiently large plane wave cutoff and local orbitals. Treating the Fe 3*s* and 3*p* semi-core states as local orbitals significantly affects the G_0W_0 results.

The calculated optical absorption within GW does not exhibit significant changes as compared to plain PBE for the first peak, both being in nice agreement with experiment.^{45,46} The second peak (i.e., peaks C and D in Fig. 4) in the optical absorption is in a better agreement with experiment using PBE. However, it may be that the second peak is caused by excitonic effects, which are not considered in our theoretical framework.

A fundamental band gap of only 0.3 eV in iron pyrite may be an explanation for its disappointing low photovoltaic performance. So far, the size of the fundamental band gap in iron pyrite is still not resolved and new experimental data of the position of the *p*-like band is highly desirable.

ACKNOWLEDGMENTS

We acknowledge funding from BMBF under the Project No. 03SF0402 (NADNuM) and the Jülich Supercomputing Centre (JSC) for computational time. Additionally, we want to thank P. Xu, C. Friedrich, I. Aguilera, E. Şaşıoğlu, M. Schlipf, G. Michalíček, and M. Betzinger for fruitful discussions.

*t.schena@fz-juelich.de

- ¹A. Ennaoui, S. Fiechter, C. Pettenkofer, N. Alonso-Vante, K. Büker, M. Bronold, C. Höpfner, and H. Tributsch, *Sol. Energy Mater. Sol. Cells* **29**, 289 (1993).
- ²S. W. Lehner, K. S. Savage, and J. C. Ayers, *J. Cryst. Growth* **286**, 306 (2006).
- ³C. Steinhagen, T. B. Harvey, C. J. Stolle, J. Harris, and B. A. Korgel, *J. Phys. Chem. Lett.* **3**, 2352 (2012).
- ⁴P. Cervantes, Z. Slanic, F. Bridges, E. Knittel, and Q. Williams, *J. Phys. Chem. Solids* **63**, 1927 (2002).
- ⁵M. Birkholz, S. Fiechter, A. Hartmann, and H. Tributsch, *Phys. Rev. B* **43**, 11926 (1991).
- ⁶M. Bronold, Y. Tomm, and W. Jaegermann, *Surf. Sci. Lett.* **314**, L931 (1994).
- ⁷R. Sun, M. K. Y. Chan, S. Y. Kang, and G. Ceder, *Phys. Rev. B* **84**, 035212 (2011).
- ⁸R. Sun, M. K. Y. Chan, and G. Ceder, *Phys. Rev. B* **83**, 235311 (2011).
- ⁹F. W. Herbert, A. Krishnamoorthy, K. J. VanVlieta, and B. Yildiz, *Surf. Sci.* **618**, 53 (2013).
- ¹⁰S. Seefeld, M. Limpinsel, Y. Liu, N. Farhi, A. Weber, Y. Zhang, N. Berry, Y. J. Kwon, C. L. Perkins, J. C. Hemminger, R. Wu, and M. Law, *J. Am. Chem. Soc.* **135**, 4412 (2013).
- ¹¹J. Hu, Y. Zhang, M. Law, and R. Wu, *Phys. Rev. B* **85**, 085203 (2012).
- ¹²J. Hu, Y. N. Zhang, M. Law, and R. Q. Wu, *J. Am. Chem. Soc.* **134**, 13216 (2012).
- ¹³Y. N. Zhang, J. Hu, M. Law, and R. Q. Wu, *Phys. Rev. B* **85**, 085314 (2012).
- ¹⁴L. Yu, S. Lany, R. Kykyneshi, V. Jieratum, R. Ravichandran, B. Pelatt, E. Altschul, H. A. S. Platt, J. F. Wager, D. A. Keszler, and A. Zunger, *Adv. Energy Mater.* **1**, 748 (2011).
- ¹⁵V. Eyert, K. H. Höck, S. Fiechter, and H. Tributsch, *Phys. Rev. B* **57**, 6350 (1998).
- ¹⁶S. G. Choi, J. Hu, L. S. Abdallah, M. Limpinsel, Y. N. Zhang, S. Zollner, R. Q. Wu, and M. Law, *Phys. Rev. B* **86**, 115207 (2012).
- ¹⁷P. Lazić, R. Armiento, F. W. Herbert, R. Chakraborty, R. Sun, M. K. Y. Chan, K. Hartman, T. Buonassisi, B. Yildiz, and G. Ceder, *J. Phys.: Condens. Matter* **25**, 465801 (2013).
- ¹⁸T. A. Bither, R. J. Bouchard, W. H. Cloud, P. C. Donohue, and W. J. Siemons, *Inorg. Chem.* **7**, 2208 (1968).
- ¹⁹A. Ennaoui, S. Fiechter, H. Goslowsky, and H. Tributsch, *J. Electrochem. Soc.* **132**, 1579 (1985).
- ²⁰P. Hohenberg and W. Kohn, *Phys. Rev.* **136**, B864 (1964).
- ²¹W. Kohn and L. J. Sham, *Phys. Rev.* **140**, A1133 (1965).
- ²²J. P. Perdew, K. Burke, and M. Ernzerhof, *Phys. Rev. Lett.* **77**, 3865 (1996).
- ²³V. I. Anisimov, F. Aryasetiawan, and A. I. Liechtenstein, *J. Phys.: Condens. Matter* **9**, 767 (1997).
- ²⁴J. P. Perdew and M. Levy, *Phys. Rev. Lett.* **51**, 1884 (1983).
- ²⁵L. J. Sham and M. Schlüter, *Phys. Rev. Lett.* **51**, 1888 (1983).
- ²⁶J. Heyd, J. E. Peralta, and G. E. Scuseria, *J. Chem. Phys.* **123**, 174101 (2005).
- ²⁷B. G. Janesko, T. M. Henderson, and G. E. Scuseria, *Phys. Chem. Chem. Phys.* **11**, 443 (2009).
- ²⁸L. Hedin, *Phys. Rev.* **139**, A796 (1965).
- ²⁹S. W. Lehner, N. Newman, M. van Schilfgaarde, S. Bandyopadhyay, K. Savage, and P. R. Buseck, *J. Appl. Phys.* **111**, 083717 (2012).
- ³⁰B. C. Shih, Y. Xue, P. Zhang, M. L. Cohen, and S. G. Louie, *Phys. Rev. Lett.* **105**, 146401 (2010).
- ³¹C. Friedrich, M. C. Müller, and S. Blügel, *Phys. Rev. B* **83**, 081101 (2011).
- ³²W. Paszkowicz and J. A. Leiro, *J. Alloys Compd.* **401**, 289 (2005).
- ³³D. J. Singh, *Planewaves, Pseudopotentials and the LAPW Method* (Kluwer-Academic, Boston, 1994).
- ³⁴<http://www.flapw.de>
- ³⁵C. Friedrich, S. Blügel, and A. Schindlmayr, *Phys. Rev. B* **81**, 125102 (2010).
- ³⁶C. Friedrich, A. Schindlmayr, S. Blügel, and T. Kotani, *Phys. Rev. B* **74**, 045104 (2006).
- ³⁷G. Michalíček, M. Betzinger, C. Friedrich, and S. Blügel, *Comput. Phys. Commun.* **184**, 2670 (2013).
- ³⁸E. Engel and R. N. Schmid, *Phys. Rev. Lett.* **103**, 036404 (2009).
- ³⁹M. Betzinger, C. Friedrich, A. Görling, and S. Blügel, *Phys. Rev. B* **85**, 245124 (2012).
- ⁴⁰A. Marini, G. Onida, and R. DelSole, *Phys. Rev. Lett.* **88**, 016403 (2001).
- ⁴¹T. Rangel, D. Kecik, P. E. Trevisanutto, G. M. Rignanese, H. VanSwygenhoven, and V. Olevano, *Phys. Rev. B* **86**, 125125 (2012).
- ⁴²P. Umari and S. Fabris, *J. Chem. Phys.* **136**, 174310 (2012).
- ⁴³C. Bradley and A. Cracknell, *The Mathematical Theory of Symmetry in Solids* (Oxford University Press, Oxford, UK, 2009).
- ⁴⁴J. Vidal, S. Botti, P. Olsson, J. F. Guillemoles, and L. Reining, *Phys. Rev. Lett.* **104**, 056401 (2010).
- ⁴⁵K. Sato, *Prog. Crystal Growth Charac.* **11**, 109 (1985).
- ⁴⁶I. J. Ferrer, D. M. Nevskaja, C. de las Heras, and C. Sánchez, *Solid State Commun.* **74**, 913 (1990).
- ⁴⁷I. J. Ferrer and C. Sánchez, *Solid State Commun.* **81**, 371 (1992).
- ⁴⁸A. Schlegel and P. Wachter, *J. Phys. C: Solid State Phys.* **9**, 3363 (1976).
- ⁴⁹S. Suga, K. Inoue, M. Taniguchi, S. Shin, M. Seki, K. Sato, and T. Teranishi, *J. Phys. Soc. Jpn.* **52**, 1848 (1983).
- ⁵⁰Equation (1) does not add up to the total optical absorption when summed up for all orbital contributions. However, using four particular energies $\hbar\omega$ and the corresponding values for the optical absorption we are able to calculate the factors for the

four orbital contributions within a system of linear equations to yield approximately the total optical absorption. So, we obtain an excellent agreement between the sum of the four orbital contributions and the total optical absorption within the range of 6 eV.

- ⁵¹P. Rinke, A. Qteish, J. Neugebauer, and M. Scheffler, *Phys. Status Solidi B* **245**, 929 (2008).
- ⁵²M. Meinert, C. Friedrich, G. Reiss, and S. Blügel, *Phys. Rev. B* **86**, 245115 (2012).
- ⁵³M. Schlipf, M. Betzinger, C. Friedrich, M. Lezaic, and S. Blügel, *Phys. Rev. B* **84**, 125142 (2011).
- ⁵⁴M. A. L. Marques, J. Vidal, M. J. T. Oliveira, L. Reining, and S. Botti, *Phys. Rev. B* **83**, 035119 (2011).
- ⁵⁵E. Sasioglu, C. Friedrich, and S. Blügel, *Phys. Rev. B* **83**, 121101 (2011).
- ⁵⁶M. Betzinger, C. Friedrich, S. Blügel, and A. Göring, *Phys. Rev. B* **83**, 045105 (2011).
- ⁵⁷P. Rinke, A. Qteish, J. Neugebauer, C. Freysoldt, and M. Scheffler, *New J. Phys.* **7**, 126 (2005).
- ⁵⁸A. N. Chantis, M. vanSchilfhaarde, and T. Kotani, *Phys. Rev. B* **76**, 165126 (2007).
- ⁵⁹N. Marom, F. Caruso, X. Ren, O. T. Hofmann, T. Körzdörfer, J. R. Chelikowsky, A. Rubio, M. Scheffler, and P. Rinke, *Phys. Rev. B* **86**, 245127 (2012).
- ⁶⁰A. Schindlmayr, T. J. Pollehn, and R. W. Godby, *Phys. Rev. B* **58**, 12684 (1998).
- ⁶¹M. Shishkin, M. Marsman, and G. Kresse, *Phys. Rev. Lett.* **99**, 246403 (2007).
- ⁶²G. Brostigen, A. Kjekshus, and C. Romming, *Acta Chem. Scand.* **27**, 2791 (1973).